Biointerface Research in Applied Chemistry
Open-Access Journal (ISSN: 2069-5837)

Article
Volume 14, Issue 6, 2024, 148
https://doi.org/10.33263/BRIAC146.148

Optical and Dielectric Properties of Magnesium Aluminate Spinel with Varying Degrees of Stoichiometry

Prabhpreet Kaur [1], Farzana Farooq [1], Suman Rani [1,*]

[1] Department of Physics, School of Chemical Engineering and Physical Sciences, Lovely Professional University, Punjab, India
* Correspondence: suman.rani@lpu.co.in;

Scopus Author ID 57614968000
Received: 11.07.2023; Accepted: 6.01.2024; Published: 13.12.2024

Abstract: This study investigated magnesium aluminate spinel's optical and dielectric properties with varying stoichiometry degrees. The nanoparticles were prepared using a wet chemical route technique, and different molar ratios of Mg/Al (1:2, 1:1, 2:1) were used to create both stoichiometric and non-stoichiometric samples. The resulting nano-powders were sintered at 1100°C, and their morphological properties were investigated using X-ray diffraction (XRD), which showed that all samples had a cubic structure. However, the crystallinity and crystallite size decreased as the Mg/Al ratio moved from 1:2 to 1:1 and then to 2:1. UV-Vis spectroscopy was used to determine the optical bandgap energy, and fluorescence spectra showed multicolored emission since the presence of various defect states in the energy gap, such as anionic, cationic, antisite, Schottky, and interstitial. The dielectric properties were studied in the 500 Hz to 1 MHz frequency range, and the calculated alternating current (AC) conductivity increased with frequency. These findings suggest that the prepared materials may be suitable for optoelectronic devices, microwave applications, and semiconductor devices.

Keywords: magnesium aluminate spinel; stoichiometric; non-stoichiometric; nanoparticles; optical properties; dielectric properties.

1. Introduction

With the advancement of scientific research, nanotechnology has emerged as a highly promising field with diverse applications. With this rapidly developing technology, there is considerable interest in materials characterized by wide bandgap, high mechanical strength, and high electrical resistivity. Recently, nanoparticles based on aluminates have gained significant attention and have been extensively investigated for their applications as luminescent and energy-storage materials [1-3]. The advancement of information technology has sparked increased interest in optoelectronic and high-performance storage devices. Magnesium aluminate spinel ($MgAl_2O_4$) (MAS) is a material that possesses the desired properties mentioned above. MAS exhibits a general formula of AB_2O_4, where A is Mg^{2+} and B is Al^{3+}, having a face-centered cubic structure within the Fd3m space group [4]. Khaidukov et al. [5] explored the utility of $MgAl_2O_4$ as a phosphor, concluding that it is a suitable material for developing various types of PC-LED lamps. Egorov et al. [6] investigated $MgAl_2O_4$ in the terahertz range and identified it as a promising material for microelectronic devices. MAS's optical and dielectric characteristics are of great significance, and these properties are highly dependent on the preparation method and chemical composition. For the fabrication of MAS

nanoparticles, various synthesis techniques are employed, including solid-state reaction [7], co-precipitation [8], auto-combustion [9], and sol-gel technique [10]. The structure of magnesium aluminate spinel is illustrated in Figure 1.

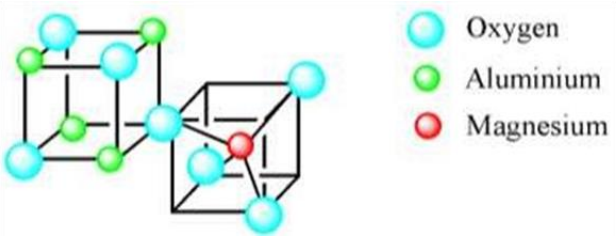

Figure 1. Structure of $MgAl_2O_4$: Mg ions occupy the tetrahedral site, while Al ions occupy the octahedral site [16].

Consequently, in the study of material properties, the initial proportion of reagents is crucial, as it significantly influences the final product. Several reports [11-14] have been published to investigate the impact of stoichiometric and non-stoichiometric molar ratios of different materials. However, for Magnesium aluminate spinel ($MgAl_2O_4$), a limited number of studies have explored variations in the molar ratios of Mg/Al. In this paper, MAS nanoparticles were synthesized using the sol-gel technique with different molar concentrations. The sol-gel technique was chosen due to its simplicity in producing high-purity materials with a homogeneous composition [15]. This study explores the influence of Mg/Al molar ratios on MAS nanoparticles' crystallite size, energy bandgap, and electrical conductivity.

2. Materials and Methods

The sol-gel wet chemical method was used to synthesize the stoichiometric (1:2) and non-stoichiometric (1:1, 2:1) magnesium aluminate spinel (MAS). Magnesium nitrate [$Mg(NO_3)_2.6H_2O$] with 98% purity having molecular weight 256.41, Aluminium nitrate [$Al(NO_3)_3.9H_2O$] with 98% purity having molecular weight 375.13, citric acid ($C_6H_8O_7H_2O$) with purity of 98% with molecular weight 192.13; all from LOBA company were used as precursors.

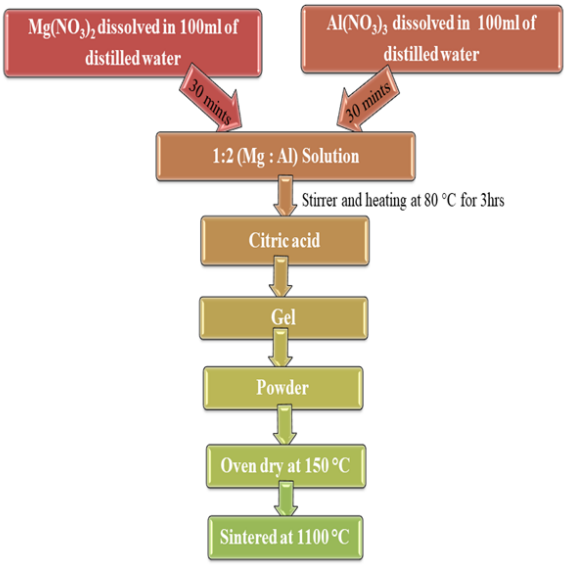

Figure 2. A simplified systematic diagram for the synthesis of stoichiometric (1:2) spinel.

Changing the molar ratio of magnesium and aluminate to 1:2, 1:1, and 2:1 allowed an appropriate amount to be dissolved in 100 ml of distilled water in two separate beakers and a stirrer for 30 minutes. The solutions were then mixed in one beaker to attain homogeneity. This solution was stirred and heated by adding citric acid until it became milky in color and formed a gel. The gel was dried on a hot plate until nano-powder formed. These prepared nano-powders were heated in a muffle furnace (±1°C) at 1100°C for 4hrs. Figure 2 depicts a simplified systematic diagram for the synthesis of stoichiometric (1:2) spinel in a simplified way. Similar procedures will be used to synthesize non-stoichiometric (1:1, 2:1) spinels.

3. Results and Discussion

3.1. X-ray diffraction (XRD).

The XRD patterns of MAS nanoparticles synthesized with three different molar ratios of Mg/Al = 1:2, 1:1, 2:1 are shown in Figure 3. As the molar ratio changes from stoichiometric ratio (2:1) to non-stoichiometric (1:1, 2:1), the formation of two phases, i.e., $MgAl_2O_4$ and MgO, starts to be observed. This occurs due to the presence of an excess of magnesium and oxygen in the lattice. The diffraction peaks show that the material has a cubic structure indexed from JCPDS no: 00-021-1152 for the $MgAl_2O_4$ phase and JCPDS no: 00-045-0946 for the MgO phase. The formation of two phases leads to affect the crystallinity of nanoparticles. The crystallinity is defined as the degree of long-range structural order that makes up a crystal lattice within a solid. As the stoichiometric ratio changes, the crystallinity of the prepared nanoparticles starts decreasing, and peak intensity decreases with the increase of full-width half maxima (FWHM). This trend is mentioned in Table 1. The Debye-Scherrer formula(equation 1) is used to calculate the average crystallite size (D) [17]:

$$D = \frac{0.94\lambda}{\beta cos\theta} \qquad (1)$$

Table 1. Calculated crystallite size, peak intensities, and bandgap of MAS with three different molar ratios.

Sample	**1:2 (Mg/Al)**	**1:1 (Mg/Al)**	**2:1 (Mg/Al)**
Crystallite Size (nm)	33.01	28.70	**28.41**
F.W.H.M. (degree)	0.23	0.27	**0.29**
Intensity (a.u.)	63.21	46.34	**35.75**
Crystallinity (%)	67.85	54.66	**42.11**
Bandgap (E_g) (eV)	**5.14**	**5.20**	**5.30**

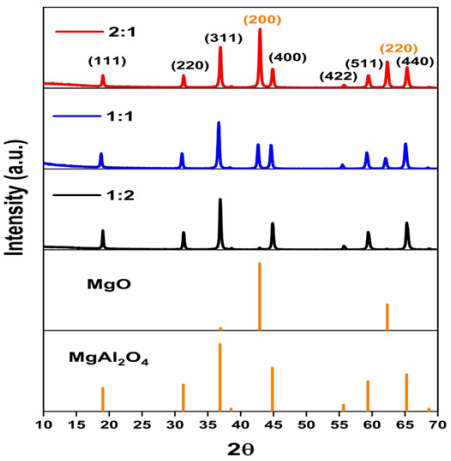

Figure 3. Powder XRD patterns of MAS synthesized with 1:2, 1:1, and 2:1 molar ratios.

3.2. Scanning electron microscopy (SEM) and energy-dispersive spectroscopy (EDS).

The SEM and EDS analysis is shown in Figure 4. The morphology and structure of the prepared nanoparticles were investigated using FESEM. It can be observed that even with the change of molar ratio, the prepared samples were uniform and well-dispersed. The SEM images also depicted that under the influence of electrostatic gravity, the uneven surface of nanoparticles gets self-aggregated into larger nanoparticles. The EDS spectra show the pattern of prepared material at different molar ratios. EDS data confirms the chemical composition and the elements present in the prepared composition are according to the desired Mg/Al molar ratio as 1:2, 1:1, and 2:1.

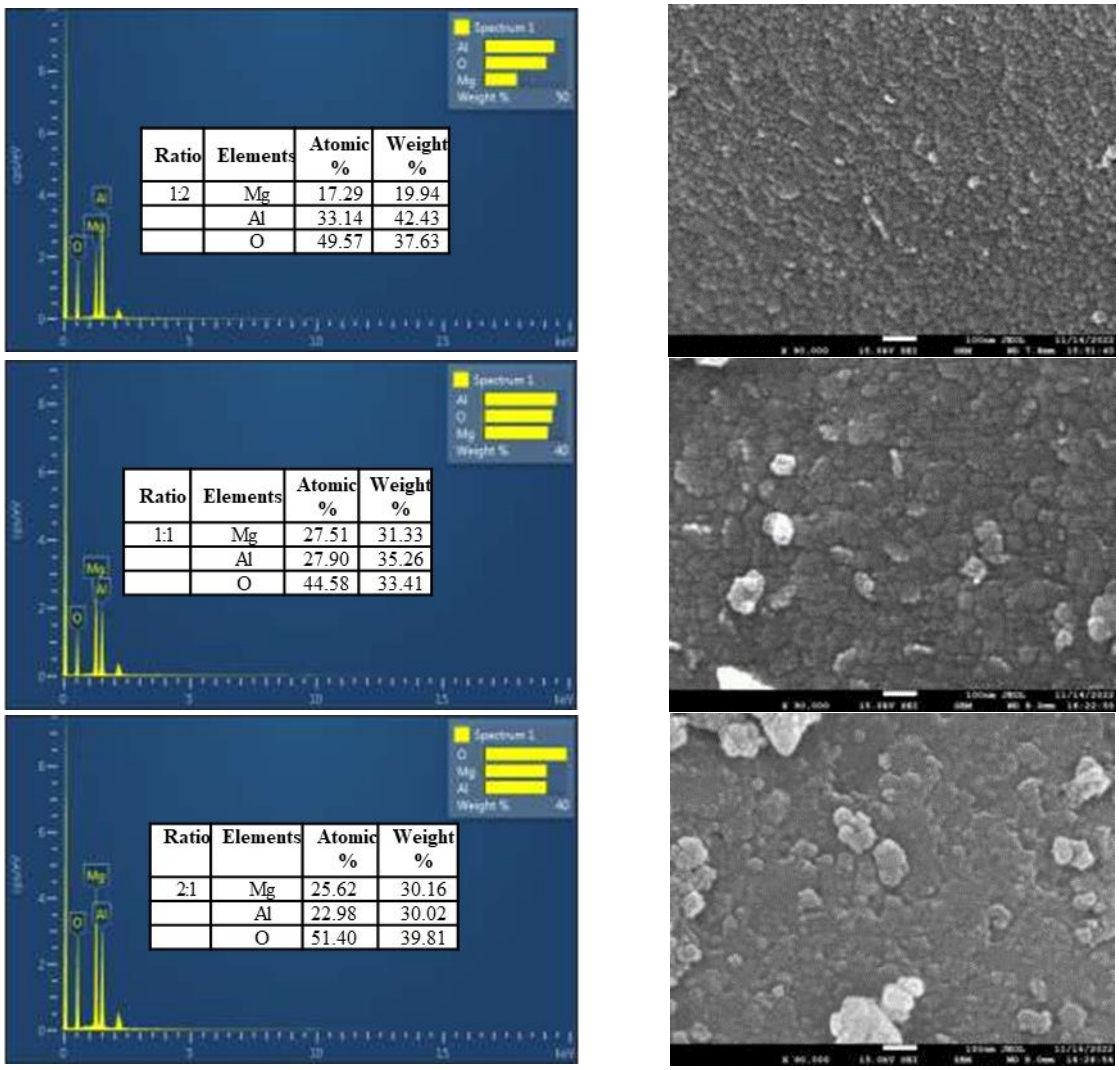

(a) **(b)**

Figure 4. Shows **(a)** Elemental analysis (EDS); **(b)** SEM images of MAS nanoparticle at 1:2, 1:1, 2:1 molar ratio.

3.3. Fourier transfer infrared (FTIR) spectroscopy.

The FTIR analysis of MAS nano-powder at three different molar ratios is depicted in Figure 5. The spectra have been recorded in the range 400-4000 cm^{-1}. The recorded spectra of all the samples showed the same absorption bands. The absorption peak at the wavenumber of 2345 cm^{-1} shows the presence of O-O bonds in the crystal lattice, a feature of spinel-structured crystallites [18]. The absorption peaks in the range of 900-450 cm^{-1} are related to the metal-oxygen-metal bonds. The peak at the wavenumber of 696 cm^{-1} is related to the stretching modes of Mg-O. In addition, the peak at 508 cm^{-1} is related to the

stretching modes of Al-O in octahedral sites. The peaks at the wavenumber of 696 cm^{-1} and 508 cm^{-1} show the formation of $MgAl_2O_4$ spinel.

On the other hand, as the ratio changes to non-stoichiometric (1:1 and 2:1), an additional peak at 827cm^{-1} starts to appear. This absorption peak indicates the presence of cubic MgO. These results are consistent with several theoretical and experimental results [19,20].

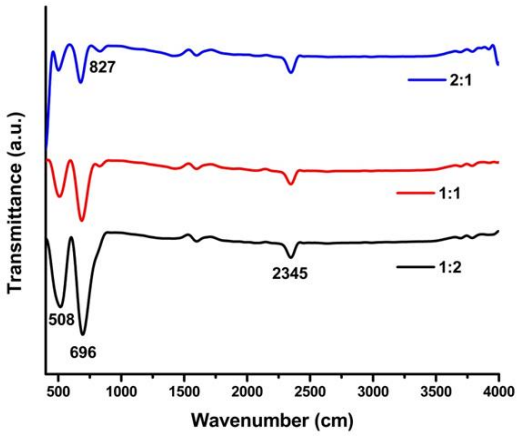

Figure 5. FTIR spectra of MAO with different molar ratios.

3.4. UV-visible spectrosocpy.

Figure 6a shows the absorption peak of MAS with Mg/Al 1:2, 1:1, and 2:1 in UV-Vis spectra ranging from 200-500 nm. The spectra show two absorption peaks at 208nm and 250 nm. The peak at 208 nm can arise from Band-to-Band absorption from $MgAl_2O_4$ related to [21]. The absorption band at 250 nm is due to the presence of F-centers. It can be noticed that the absorption edge cannot be affected by changing the molar ratios. It is observed that the intensity of the absorption decreases by changing the stoichiometric ratio. Figure 6b demonstrates the value of the optical bandgap by extrapolating the linear region of E_g v/s $(\alpha h\upsilon)^2$ plot. The energy bandgap value is estimated from Tauc's description in equation 2 [22]

$$(\alpha h\upsilon)^2 = A(h\upsilon - Eg) \qquad (2)$$

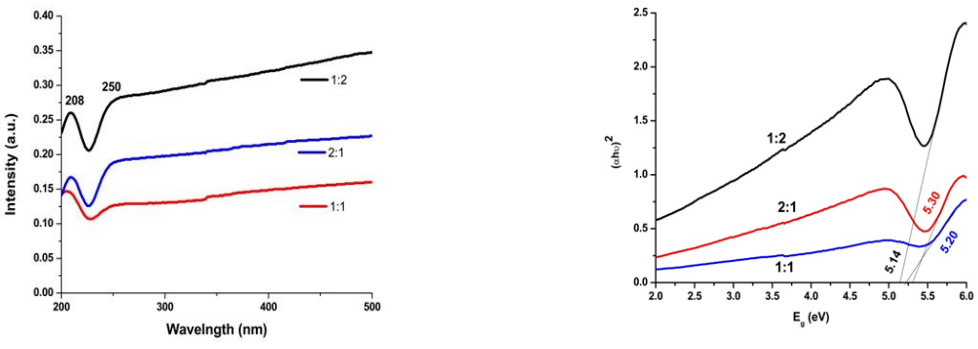

(a) **(b)**

Figure 6. (**a**) UV-visible spectra of prepared material; (**b**) calculated value of bandgap.

Where E_g is energy bandgap; υ is the frequency of light; h is Planck's constant; A refers to the proportionality constant; α is the absorption coefficient. The estimated value of bandgap is 5.14eV, 5.20eV, and 5.30eV with a Mg/Al molar ratio of 1:2, 1:1, and 2:1, respectively. It was determined that the bandgap increases as the molar ratios of the Mg^{2+}

cation increase. The relation between crystallite size and optical bandgap with different molar ratios is plotted in Figure 7. The graph reveals that the crystallite size decreases with an increase in the bandgap of the material. The obtained results are consistent with quantum confinement theory [23], which asserts that electrons and holes in the conduction band (CB) and valence band (VB) are confined by the potential barriers of the surface or potential well of the quantum box. Because of this confinement, the energy gap (E_g) between the CB and VB increases as the particle size decreases—however, Figure 8 exhibits color images of prepared nanoparticles under three different light sources.

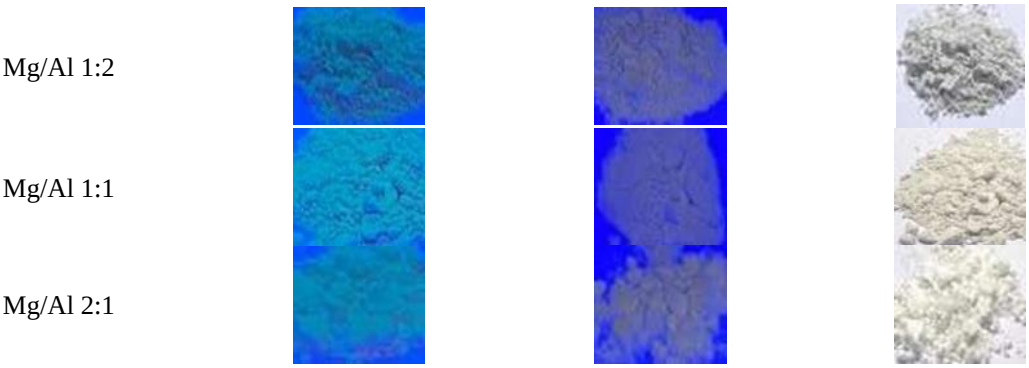

Figure 8. Sample under: (**a**) low UV region; (**b**) High UV region; (**c**) Visible region.

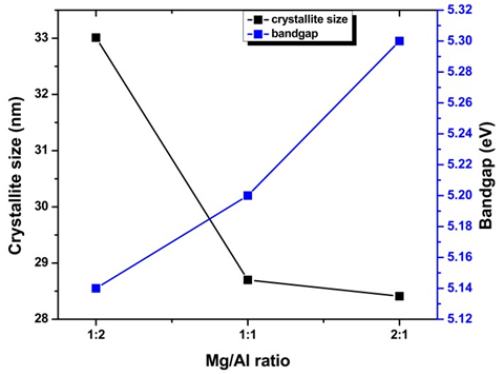

Figure 7. Relation between crystallite size and bandgap with different molar ratios.

3.5. Fluorescence spectroscopy(FS).

The emission spectra of MAS at molar ratios 1:2, 1:1, and 2:1 are shown in Figure 9. The nanophosphors have given two excitations of 209 nm and 250 nm as the material exhibits maximum absorption in these regions, as shown in the UV absorption spectrum Figure 6a. The emission spectra were recorded in the region from 400-800 nm. It is observed that at both the excitation wavelengths, the material shows broad emission in the blue region. This broad emission reveals the presence of different defect states in the MAS bandgap [24]. The emission peak at approximately 440nm is caused by the charge transfer between Al^{3+} and its surrounding O^{2-} ions. Another broad peak, approximately at 650nm, is caused by the presence of oxygen vacancies [25]. Figure 10 shows the bar graph with integrated intensities versus excitation wavelength at 1:2, 1:1, and 2:1 molar ratios. The graph shows that as the excitation wavelength increases, the intensity decreases. The presence of more F-centers could explain this increase in intensity at lower excitation levels.

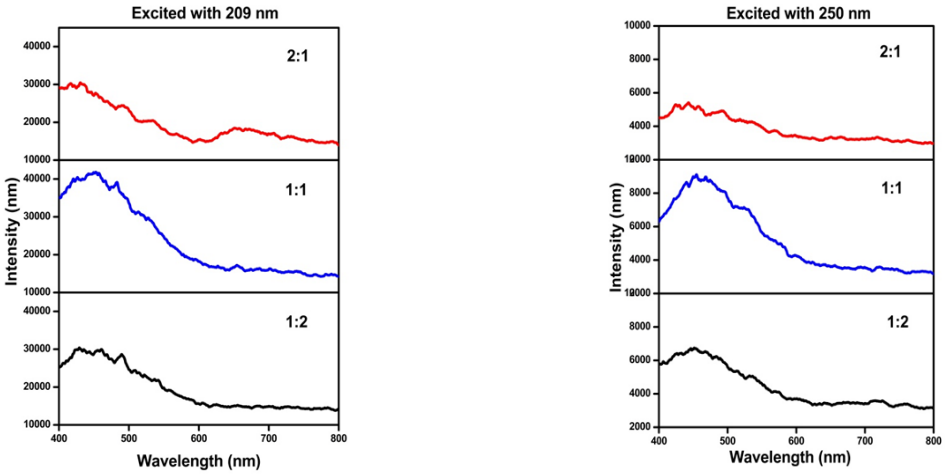

(a) **(b)**

Figure 9. Emission spectra of MAO at different molar ratios (1:2, 1:1, 2:1): **(a)** excited with 209 nm; **(b)** excited with 250 nm.

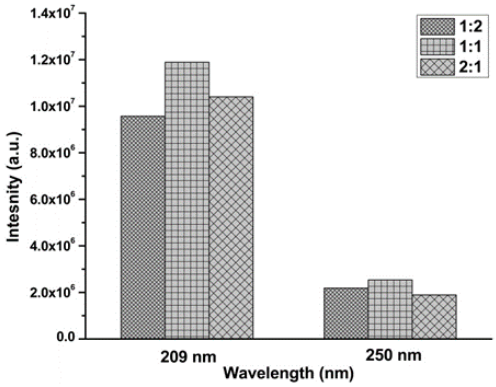

Figure 10. Intensity v/s wavelength graph of Mg/Al molar ratios.

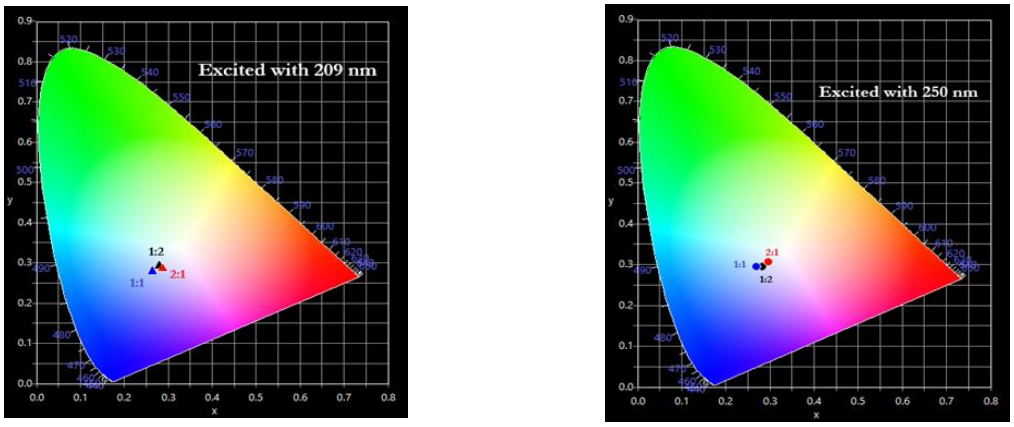

(a) (b)

Figure 11. CIE coordinates of prepared material at **(a)** 209 nm; **(b)** 250 nm.

Table 2. CIE, CCT, CP, and CRI values of prepared nano-powder.

Sample	**Excitations 209nm**				**Excitation 250nm**			
	CIE	**CCT**	**Color Purity (%)**	**CRI**	**CIE**	**CCT**	**Color Purity (%)**	**CRI**
1:2	(0.280, 0.292)	9856	17.6	98	(0.282, 0.294)	9487	17.0	98
1:1	(0.264, 0.279)	13099	22.4	99	(0.268, 0.293)	11064	19.8	96
2:1	(0.287, 0.285)	9380	22.7	89	(0.297, 0.306)	7825	34.3	89

To denote specifically the color characterization of the MAS compound, the International Commission on Illumination (CIE) coordinates, correlated color temperature

(CCT), color purity (CP), and color rendering index (CRI) were evaluated and shown in Table 2. The CIE coordinates are mentioned in Figure 11 by using the chromaticity diagram.

The value of CCT can be calculated by using

$$CCT = -449n^3 + 3525n^2 - 6823.3n + 5520.33 \quad (3)$$

where $=\frac{x-x_i}{y-y_i}$ The quantity ―color purity‖ describes how pure or monochromatic a color is at a given light. The value of color purity lies between 0 to 100. For ideal white light, color purity is zero. The color purity can be evaluated by using the equation described in [26]. The calculated value of color purity at two different excitations is mentioned in Table 2. From these values, it is concluded that MAS at a 1:2 molar ratio has suitable color purity compared to others.

CRI measures how accurately a light source can replicate various objects' colors compared to a natural light source. When the light source performs exactly like natural light, the CRI rating is ―100 [27]. From the calculated results of CIE coordinates, CRI, and color purity, it is observed that among the three different ratios, 1:2 is best suited for exploring the luminescence properties of MAS spinel. This shows that the prepared material is suitable for optoelectronic devices. Moreover, these results can be further improved with proper dopant to target the suitable application area.

3.6. Dielectric properties.

Impedance analysis is a powerful method for determining the relationship between the dielectric properties of synthesized material and its microstructural composition [28]. The real and imaginary impedance parts are determined for each spinel MAS sample at Mg/Al = 1:2, 1:1, 2:1 molar ratio in the 500 Hz to 1 GHz frequency range at room temperature.

3.6.1. Real and imaginary impedance.

The real and imaginary parts of prepared spinels having the composition of MAO (1:2, 1:1, 2:1) are shown in Figure 12. The real and imaginary part w.r.t. frequency is calculated for each sample. The graph shows that these impedance parts depend upon the applied frequency.

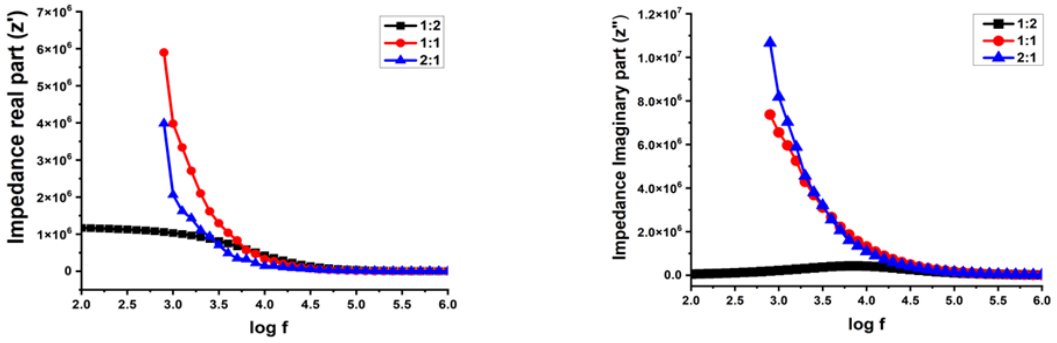

(a) **(b)**

Figure 12. This figure shows the (**a**) real; (**b**) imaginary part of impedance on the y-axis versus the log of frequency on the x-axis.

3.6.2. Nyquist plot.

The Nyquist plot offers a helpful method for separating grain resistance from grain boundaries. The Nyquist plot, with Z′ along the x-axis and Z" along the y-axis, is shown

in Figure 13. From this plot, we can infer three separate electroactive zones. These areas include the interface between the samples and the electrodes, the insulating grain borders, and the conducting grain boundaries. According to the current investigation, each specimen had a semicircle that matched the grain boundaries and actively contributed to the electrical properties of prepared samples. The diameter of a semicircle and the specimen's resistance are directly related [30]. It is evident that the diameter of the semicircle decreases when the Mg/Al ratio approaches 1:2. This drop in diameter represents the increase in conductivity and decrease in resistivity. The variation in the radius of the semicircle may be due to the change in molar concentration from stoichiometric to non-stoichiometric ratio.

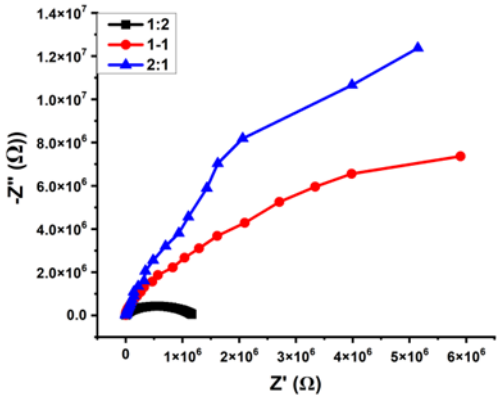

Figure 13. Nyquist plot with changing molar ratio.

3.6.3. Frequency-dependent A.C. conductivity.

The value for the AC conductivity of the Mg/Al=1:1, 2:1, 1:2 can be calculated using [31] (σ_{ac})

$$\sigma_{ac} = 2\pi f \varepsilon_0 \varepsilon' tan\delta \qquad (4)$$

Where ε', f, and ε_o represent the real part of free space's dielectric constant, frequency, and permittivity. The graph of AC conductivity and log of frequency is shown in Figure 14. The material showed resistive behavior in the low-frequency region due to the grain boundaries. At high frequencies, the material's conductivity gets enhanced due to the hopping of charge carriers [31]. The AC conductivity of 1:2 (Mg/Al) is observed to be higher than others. In the 1:2 (Mg/Al) sample, there are more hopping phenomena between the tetrahedral and octahedral sites than others, leading to the sample's conductive nature. Similar results have been found in previous research [32], which concluded that the 1:2 ratio (stoichiometric spinel) produced the best performance even by varying the stoichiometric ratio.

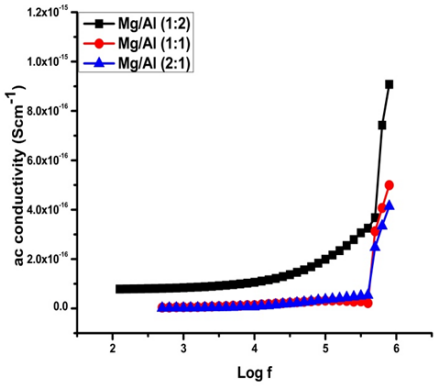

Figure 14. AC conductivity versus the log of frequency.

4. Conclusions

Magnesium aluminate spinel (MAS) at 1:2, 1:1, and 2:1 molar ratios were successfully synthesized using the wet chemical sol-gel method sintered at 1100°C in a muffle furnace (±1°C). The collective study of characterizations was used to study the phase formation, surface morphology, chemical composition, and luminescence study. A comprehensive characterization study covering X-ray diffraction (XRD), scanning electron microscopy (SEM), energy-dispersive X-ray spectroscopy (EDS), UV-Vis spectroscopy, and fluorescence spectroscopy (FL) was conducted to explain the phase formation, surface morphology, chemical composition, and luminescent properties. XRD analysis revealed that MAS, with a 1:2 molar ratio, exhibited a single phase of $MgAl_2O_4$. Conversely, a shift to molar ratios of 1:1 and 2:1 introduced two phases, MgO and $MgAl_2O_4$, resulting in decreased nano-powder crystallinity. Fluorescence spectra exhibit emissions at 209 nm and 250 nm under UV excitation. The emission spectra of all samples show the highest peak, approximately 440 nm, due to the charge transition between Al^{3+} and its surrounding O^{2-} ions. The excitation of 209 nm is best suited because it can give high integral intensity. Consequently, from three different molar ratios, 1:2 is best optimized with CIE coordinates (0.2800, 0.2922), color purity (17.6), and CRI (98). The frequency-dependent conductivity was measured and analyzed at room temperature by varying the Mg/Al molar ratios. The observed results are reported. The results highlight that MAS, especially at a 1:2 molar ratio, is promising for optoelectronic devices due to its customized optical and electrical properties. Additionally, enhancements can be achieved by introducing appropriate dopants to address suitable application requirements.

Funding

This research received no external funding.

Acknowledgments

Presented at the 4th International Conference on Recent Advances in Fundamental and Applied Sciences (RAFAS-2023) on March 24-25, 2023, organized by the School of Chemical Engineering and Physical Sciences, Lovely Professional University, Punjab, India.

Conflicts of Interest

The authors declare no conflict of interest.

References

1. Ziva, A.Z.; Suryana, Y.K.; Kurniadianti, Y.S.; Nandiyanto, A.B.D.; Kurniawan, T. Recent Progress on the Production of Aluminum Oxide (Al2O3) Nanoparticles: A Review. *Mech. Eng. Soc. Ind.* **2021**, *1*, 54–77, http://doi.org/10.31603/mesi.5493.
2. Samal, P.; Vundavilli, P.R.; Meher, A.; Mahapatra; M.M. Recent progress in aluminum metal matrix composites: A review on processing, mechanical and wear properties. *J. Manuf. Process.* **2020**, *59*, 131–152, http://doi.org/10.1016/j.jmapro.2020.09.010.
3. Benkhelif, A.; Kolli, M. Synthesis of Pure Magnesium Aluminate Spinel ($MgAl_2O_4$) from Waste Aluminum Dross. *Waste Biomass Valor*. **2022**, *13*, 2637–2649, http://doi.org/10.1007/s12649-022-01677-1.
4. Murphy, S.T.; Gilbert, C.A.; Smith, R.; Mitchell, T.E.; Grimes, R.W. Non-stoichiometry in $MgAl_2O_4$ spinel.

Philos. Mag. **2010**, *90*, 1297–1305, http://doi.org/10.1080/14786430903341402.
5. Khaidukov, N.M.; Brekhovskikh, M.N.; Kirikova, N.Y.; Kondratyuk, V.A.; Makhov, V.N. Luminescence of $MgAl_2O_4$ and $ZnAl_2O_4$ spinel ceramics containing some 3d ions. *Ceram. Int.* **2020**, *46*, 21351–21359, http://doi.org/10.1016/j.ceramint.2020.05.231.
6. Egorov, S.V.; Sorokin, A.A.; Ilyakov, I.E.; Shishkin, B.V.; Serov, E.A.; Parshin, V.V.; Rybakov, K.I.; Balabanov, S.S.; Belyaev, A.V. Terahertz Dielectric Properties of Polycrystalline $MgAl_2O_4$ Spinel Obtained by Microwave Sintering and Hot Pressing. *J. Infrared Milli. Terahz. Waves* **2019**, *40*, 447–455, http://doi.org/10.1007/s10762-019-00582-4.
7. Khademinia, S.; Salehi, M.; Parvarinezhad, S. Solid state synthesis of MgAl2O4 nanomaterials and solar light-induced photocatalytic removal of Malachite Green. *Int. J. Nano Dimens.* **2019**, *10*, 89–104.
8. Nam, S.; Lee, M.; Kim, B.-N.; Lee, Y.; Kang, S. Morphology controlled Co-precipitation method for nanostructured transparent $MgAl_2O_4$. *Ceram. Int.* **2017**, *43*, 15352–15359, http://doi.org/10.1016/j.ceramint.2017.08.075.
9. Mahi, K.; Mostefa, R. Characterization of Magnesium/Barium Aluminates Spinel Synthesized by Sol-Gel Auto-Combustion Method. *J. Nano- Electron. Phys.* **2022**, *14*, 02025, http://doi.org/10.21272/jnep.14(2).02025.
10. Sanjabi, S.; Obeydavi, A. Synthesis and characterization of nanocrystalline $MgAl_2O_4$ spinel via modified sol-gel method. *J. Alloys Compd.* **2015**, *645*, 535–540, http://doi.org/10.1016/j.jallcom.2015.05.107.
11. Birajdar, S.D.; Shinde, A.B.; Kadam, G.B.; Kshirsagar, P.M.; Sarnaik, M.N.; Jadhav, K.M. Effect of molar concentration variation on the crystallite size and energy band gap of CdS nanoparticles synthesized by wet chemical route. *Int. J. Adv. Res. Basic Appl. Sci.* **2015**, *2*, 74-77.
12. Awasthi, R.R.; Asokan, K.; Das, B. Effect of molar concentration on structural, magnetic domain and optical properties of $BiFeO_3$ thin films. *Appl. Phys. A.* **2019**, *125*, 338, http://doi.org/10.1007/s00339-019-2560-6.
13. Qu, H.; Cao, L.X.; Su, G.; Liu, W.; Sun, Y.G.; Dong, B.H. ZnS:Ag Luminescent Nanoparticles Synthesized with Different Molar Ratio of S/Zn. *Adv. Mater. Res.* **2009**, *79*, 589–592, http://doi.org/10.4028/www.scientific.net/AMR.79-82.589.
14. Yao, Y.; Hu, S.; Zhang, Y. A novel $MgAl_2O_4$/MgO ceramic core with water-collapsibility. *Mater. Lett.* **2022**, *306*, 130810, http://doi.org/10.1016/j.matlet.2021.130810.
15. Bokov, D.; Jalil, A.T.; Chupradit, S.; Suksatan, W.; Ansari, M.J.; Shewael, I.H.; Valiev, G.H.; Kianfar, E. Nanomaterial by Sol-Gel Method: Synthesis and Application. *Adv. Mater. Sci. Eng.* **2021**, *2021*, 5102014, http://doi.org/10.1155/2021/5102014.
16. Ganesh, I. A review on magnesium aluminate ($MgAl_2O_4$) spinel: synthesis, processing and applications. *Int. Mater. Rev.* **2013**, *58*, 63–112, http://doi.org/10.1179/1743280412Y.0000000001.
17. Varbar, M.; Alavi-Amleshi, S.M.; Rezaei, M.; Akbari, E. Catalytic Oxidation of Lean Methane over Ni/$MgAl_2O_4$ Synthesized by a Novel and Facile Mechanochemical Preparation Method. *Combust. Sci. Technol.* **2023**, 195, 1819-1839, http://doi.org/10.1080/00102202.2021.2004403.
18. Motloung, S.V.; Dejene, B. F.; Kroon, R.E.; Swart, H.C.;Ntwaeaborwa O. M. Radiative energy transfer in ZnAl2O4:0.1% Ce3+, x% Eu3+ nanophosphor synthesized by sol–gel process. *Phys. Rev. B Condens. Matter.* **2015**,468-469,11-20, http://doi.org/10.1016/j.physb.2015.04.007.
19. Milani, S.S.; Kakroudi, M.G.; Vafa, N.P.; Rahro, S.; Behboudi, F. Synthesis and characterization of $MgAl_2O_4$ spinel precursor sol prepared by inorganic salts. *Ceram. Int.* **2021**, *47*, 4813–4819, http://doi.org/10.1016/j.ceramint.2020.10.051.
20. Ewais, E.M.M.; El-Amir, A.A.M.; Besisa, D.H.A.; Esmat, M.; El-Anadouli, B.E.H. Synthesis of nanocrystalline MgO/$MgAl_2O_4$ spinel powders from industrial wastes. *J. Alloys Compd.* **2017**, *691*, 822–833, http://doi.org/10.1016/j.jallcom.2016.08.279.
21. Goswami, B.; Rani, N.; Vats, R.; Bhukkal, C.; Ahlawat, R. Highly crystalline and narrow bandgap $MgAl_2O_4$: Synthesis and characterization. In ADVANCED MATERIALS AND RADIATION PHYSICS (AMRP-2020): 5th National e-Conference on Advanced Materials and Radiation Physics, Longowal, India, 9-11 November 2020; AIP Conference Proceedings, **2021**, 2352, 020045, http://doi.org/10.1063/5.0052473.
22. Dlamini, C.; Mhlongo, M.R.; Koao, L.F.; Motaung, T.E.; Hlatshwayo, T.T.; Motloung, S.V. The effects of varying the annealing period on the structure, morphology and optical properties of $MgAl_2O_4$:0.1% Mn^{2+} nanophosphors. *Appl. Phys. A* **2020**, *126*, 75, http://doi.org/10.1007/s00339-019-3248-7.
23. Shehata, M.M.; Waly, S.A.; Abdelaziz, Y.A. Effect of Gd^{3+} doping on structural and optical properties of MgO–$MgAl_2O_4$ nanocomposites synthesized via co-precipitation method. *J. Mater. Sci. Mater. Electron.* **2021**, *32*, 7423–7430, http://doi.org/10.1007/s10854-021-05455-y.

24. Buerkle, M.; Lozac'h, M.; Mariotti, D.; Švrček, V. Quasi-band structure of quantum-confined nanocrystals. *Sci. Rep.* **2023**, *13*, 4684, http://doi.org/10.1038/s41598-023-31989-8.
25. Ahlawat, R.; Goswami, B.; Rani, N.; Rani, G. Morphological and Photophysical Tempering in Spinel $MgAl_2O_4$ Synthesized by a Novel Citrate Route Via a Suitable Annealing Scheme. *J. Electron. Mater.* **2023**, *52*, 1908–1926, http://doi.org/10.1007/s11664-022-10131-w.
26. Pathak, N.; Ghosh, P.S.; Gupta, S.K.; Mukherjee, S.; Kadam, R.M.; Arya, A. An Insight into the Various Defects-Induced Emission in $MgAl_2O_4$ and Their Tunability with Phase Behavior: Combined Experimental and Theoretical Approach. *J. Phys. Chem. C* **2016**, *120*, 4016–4031, http://doi.org/10.1021/acs.jpcc.5b11822.
27. Meza-Rocha, A.N.; Speghini, A.; Franchini, J.; Lozada-Morales, R.; Caldiño, U. Multicolor emission in lithium-aluminum-zinc phosphate glasses activated with Dy^{3+}, Eu^{3+} and Dy^{3+}/Eu^{3+}. *J. Mater. Sci. Mater. Electron.* **2017**, *28*, 10564–10572, http://doi.org/10.1007/s10854-017-6830-9.
28. Hussain, N.; Ayoub, I.; Mushtaq, U.; Sehgal, R.; Rubab, S.; Sehgal, R.; Swart, H.C.; Kumar, V. 1 - Introduction to phosphors and luminescence. In Rare-Earth-Activated Phosphors; Dubey, V., Dubey, N., Domańska, M.M., Jayasimhadri, M., Dhoble, S.J., Eds.; Elsevier, **2022**; 3-41, http://doi.org/10.1016/B978-0-323-89856-0.00008-0.
29. Yamada, Y. Dielectric Properties of Textile Materials: Analytical Approximations and Experimental Measurements—A Review. *Textiles* **2022**, *2*, 50–80, http://doi.org/10.3390/textiles2010004.
30. Joshi, J.H.; Kanchan, D.K.; Joshi, M.J.; Jethva, H.O.; Parikh, K.D. Dielectric relaxation, complex impedance and modulus spectroscopic studies of mix phase rod like cobalt sulfide nanoparticles. *Mater. Res. Bull.* **2017**, *93*, 63–73, http://doi.org/10.1016/j.materresbull.2017.04.013.
31. Sheikh, F.A.; Khalid, M.; Shifa, M.S.; Asghar, H.M.N.u.H.K.; Aslam, S.; Perveen, A.; Rehman, J.u.; Khan, M.A.; Gilani, Z.A. Effects of bismuth on structural and dielectric properties of cobalt-cadmium spinel ferrites fabricated via micro-emulsion route. *Chinese Phys. B* **2019**, *28*, 088701, http://doi.org/10.1088/1674-1056/28/8/088701.
32. Ullah, F.; Qureshi, M.T.; Sultana, K.; Saleem, M.; Elaimi, M.A.; Hameed, R.A.; Haq, S.u.; Ismail, H.S.; Anwar, M.S. Structural and dielectric studies of $MgAl_2O_4$–TiO_2 composites for energy storage applications. *Ceram. Int.* **2021**, *47*, 30665–30670, http://doi.org/10.1016/j.ceramint.2021.07.244.
33. Xuan, S.; Tian, Y.; Kong, X.; Hao, J.; Wang, X. Effect of different MgO/Al_2O_3 ratios on microstructural densification, sintering process and mechanical property of $MgAl_2O_4$ materials. *J. Mater. Res. Technol.* **2023**, *25*, 2518–2526, http://doi.org/10.1016/j.jmrt.2023.06.044.